

Photoluminescence Properties, Molecular Structures, and Theoretical Study of Heteroleptic Silver(I) Complexes Containing Diphosphine Ligands

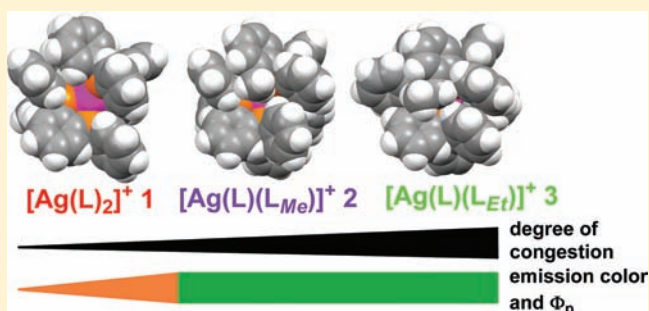
Satoshi Igawa,^{†,‡} Masashi Hashimoto,^{†,‡} Isao Kawata,^{†,§} Mikio Hoshino,[†] and Masahisa Osawa^{*,†}

[†]Luminescent Materials Laboratory, RIKEN (The Institute of Physical & Chemical Research), Hirosawa 2-1, Wako-shi 351-0198, Japan

[‡]Device Technology Development Headquarters and [§]Analysis Technology Center, Canon Incorporated, Ohta-ku, Tokyo 146-8501, Japan

Supporting Information

ABSTRACT: The homoleptic complex $[\text{Ag}(\text{L})_2]\text{PF}_6$ (**1**) and heteroleptic complexes $[\text{Ag}(\text{L})(\text{L}_{\text{Me}})]\text{BF}_4$ (**2**) and $[\text{Ag}(\text{L})(\text{L}_{\text{Et}})]\text{BF}_4$ (**3**) [L = 1,2-bis(diphenylphosphino)benzene, L_{Me} = 1,2-bis[bis(2-methylphenyl)phosphino]benzene, and L_{Et} = 1,2-bis[bis(2-ethylphenyl)phosphino]benzene] were synthesized and characterized. X-ray crystallography demonstrated that **1**–**3** possess tetrahedral structures. Photophysical studies and time-dependent density functional theory calculations of **1**–**3** revealed that alkyl substituents at the ortho positions of peripheral phenyl groups in the diphosphine ligands have a significant influence on the energy and intensity of phosphorescence of the complex in solution at room temperature. The results can be interpreted in terms of the geometric preferences of each complex in the ground and excited states. The homoleptic complex **1** exhibits weak orange phosphorescence in solution arising from its flat structure in the triplet state, while heteroleptic complexes **2** and **3** show strong green phosphorescence from triplet states with tetrahedral structure. Larger interligand steric interactions in **2** and **3** caused by their bulkier ligands probably inhibit geometric relaxation within the excited-state lifetimes, leading to higher energy phosphorescence than that observed for **1**. NMR experiments revealed that **2** and **3** in solution possess structures that are much more immobilized than that of **1**; fluxional motion is completely suppressed in **2** and **3**. Accordingly, conformational changes of **2** and **3** are expected to be suppressed by the alkyl substituents not only in the ground state but also in excited states. Consequently, nonradiative decay of the excited states of **2** and **3** occurs less efficiently than in **1**. As a result, the quantum yields of phosphorescence for **2** and **3** are 6 times larger than that for the homoleptic complex **1**.



INTRODUCTION

A number of d^{10} coinage metal complexes that exhibit interesting luminescence properties have been synthesized.¹ With regard to silver complexes, most reported to date are multinuclear complexes that have argentophilic bonding, an analogue of aurophilic bonding known as “closed-shell (d^{10} – d^{10}) interactions”.² Luminous mononuclear silver complexes, however, had rarely been reported until recently.³ In previous papers, we reported luminescence from the tetrahedral silver complex $[\text{Ag}(\text{dppb})_2]\text{PF}_6$ [**1**; dppb = 1,2-bis(diphenylphosphino)benzene (L)].^{3a} This complex exhibits an efficient phosphorescence performance in frozen 2-methyltetrahydrofuran (2-MeTHF) at 77 K: the maximum wavelength of phosphorescence $\lambda_{\text{max}} = 441$ nm, and the phosphorescence quantum yield $\Phi_{\text{p}} = 0.88$. However, this complex shows weakened phosphorescence in solution at room temperature, resulting from structural distortion in the excited state from tetrahedral to planar geometry because of the metal-

to-ligand charge-transfer (MLCT) character of the excited state. While the d^{10} ground state possesses D_{2d} symmetry, the MLCT excited state favors D_2 symmetry. The change in the structure of the triplet state results in both a red shift of λ_{max} and a decrease in Φ_{p} , with $\lambda_{\text{max}} = 670$ nm and $\Phi_{\text{p}} = 0.05$ in 2-MeTHF at ambient temperature. This phenomenon can be explained by the rigidochromic effect,^{4,5} as is frequently seen in some copper(I) complexes.⁵

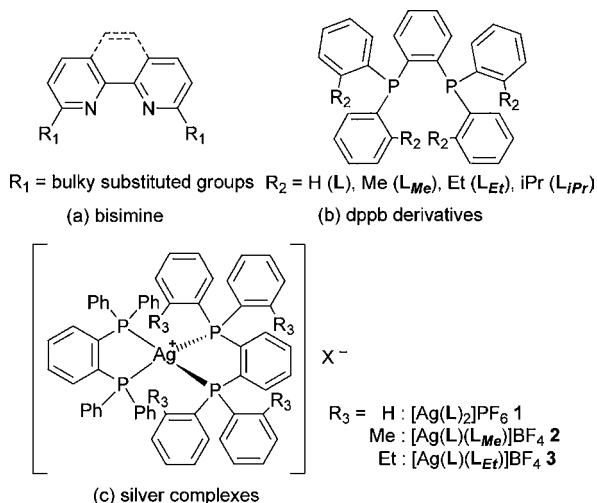
According to the extensive chemistry of tetrahedral copper(I) complexes with two diimine ligands,⁶ the incorporation of bulky substituents into diimine ligands on the side of the metal center is an effective means to prevent structural relaxation and maintain a good phosphorescence performance even in solution at room temperature. For instance, sterically congested alkyl substituents are generally introduced at the 2 and 9

Received: February 14, 2012

Published: April 30, 2012

positions of phenanthroline (or the 6 and 6' positions of 2,2'-bipyridine) to attain high Φ_{pr} as shown in Chart 1a.

Chart 1. Ligands and Silver Complexes



In line with this approach used for copper(I) diimine complexes, we have prepared diphosphine ligands in the form of dppb derivatives with substituents [Me (L_{Me}), Et (L_{Et}), and *i*Pr (L_{iPr})] at the ortho positions of four peripheral phenyl groups to afford rigid environments around the metal center in their silver(I) complexes (Chart 1b). Heteroleptic silver(I) complexes [Ag(L)(L_{Me})]BF₄ (2) and [Ag(L)(L_{Et})]BF₄ (3) were readily synthesized using dppb derivatives (Chart 1c). The steric effects of bulky substituents at the ortho positions have been briefly described in a previous paper on three-coordinate copper(I) complexes with L_{Me} .⁷ ¹H and ³¹P{¹H} NMR experiments confirmed that heteroleptic silver(I) complexes 2 and 3 were stable and did not show ligands scrambling in solution.

The photophysical properties of the dppb derivatives 2 and 3 are discussed on the basis of molecular orbital (MO) calculations, and the ability of the dppb derivatives to prevent flattening distortion through steric protection is described in detail.

EXPERIMENTAL SECTION

Chemicals. 1,2-Bis(dichlorophosphino)benzene and magnesium were obtained from Wako Pure Chemical Industries, Ltd. (2-Methylphenyl)magnesium bromide was purchased from Sigma-Aldrich. Silver(I) tetrafluoroborate, silver(I) hexafluorophosphate, (2-bromoethyl)benzene, and (2-isopropylphenyl)benzene were obtained from TCI Co., Ltd. Iodine and magnesium were purchased from Kanto Chemical Co., Inc.

General Information. All synthetic reactions were carried out under an atmosphere of argon unless otherwise indicated. ¹H, ¹³C, and ³¹P NMR spectra were recorded on a Bruker AVANCE-500 spectrometer. ¹H and ¹³C chemical shifts were referenced to residual solvent peaks. ³¹P chemical shifts were referenced to external 85% phosphoric acid ($\delta = 0$ ppm). Electrospray ionization mass spectrometry (ESI-MS) spectra were recorded on a ThermoQuest Finnigan LCQ Duo mass spectrometer. Elemental analyses (C and H) were carried out with a Vario EL CHNOS elemental analyzer from Elementar Analytical, and quantitative analyses of phosphorus for L_{Me} , L_{Et} , and L_{iPr} were performed at the Advanced Technology Support Division of RIKEN Advanced Science Institute. For emission studies, dissolved oxygen was removed by repeated freeze–pump–thaw cycles. Steady-state absorption and emission spectra were recorded at room

temperature and 77 K using a Hitachi U-3010 spectrophotometer and a Hitachi F-7000 spectrofluorometer, respectively. The light-intensity distribution of a xenon lamp incorporated in the spectrofluorometer was corrected using Rhodamine B in ethylene glycol. The output of the photomultiplier was calibrated in the wavelength range of 300–850 nm using a secondary standard lamp. Absorption spectra were measured at 77 K using a specially constructed low-temperature quartz Dewar with four optical windows. The absorption coefficient of the complexes in 2-MeTHF at 77 K was calculated on the assumption that the density of 2-MeTHF was 1.06 g/mL. Laser photolysis studies were carried out using a Nd:YAG laser (Sure Light 400, Hoya Continuum Ltd.) equipped with second-, third-, and fourth-harmonic generators. The excitation light used for emission lifetime measurements was the third harmonic (355 nm). The duration and energy of the laser pulse were 5 ns and 30 mJ/pulse, respectively. The system used to monitor the decay of emission has been reported elsewhere.⁸ Emission quantum yields in solution at room temperature and 77 K were determined with an absolute photoluminescence (PL) quantum yield measurement system (C-9920-02G, Hamamatsu).⁹ Electrochemical measurements were obtained with an electrochemical analyzer (ALS/CHI, model 600A) equipped with a single-compartment cell under an argon atmosphere. A glassy carbon electrode and coiled platinum wire were used as the working and counter electrodes, respectively. The reference electrode was Ag/AgNO₃ in CH₃CN, and the scan rate was 100 mV/s. Sample solutions were prepared by dissolving a sample (1 mM) in an electrolyte solution of [(Bu)₄N][PF₆] in CH₃CN (0.1 M, 8 mL). The reference electrode was calibrated before measurements using an external ferrocene standard.

Crystal Structure Determination. The crystallographic data and the results of structure refinements are summarized in Table S1 in the Supporting Information (SI). In the reduction of data, Lorentz and polarization corrections and empirical absorption corrections were made. The structures were solved by direct methods (SIR2004).¹⁰ All non-hydrogen atoms were refined with anisotropic thermal parameters. Hydrogen atoms were fixed at calculated positions. The X-ray crystallographic data of 1 have been reported previously.^{3a} CCDC reference numbers are 756865 for 1, 865271 for 2, and 865272 for 3.

Computational Details. Optimization of the geometries of the singlet ground (S_0) and lowest triplet excited (T_1) states in tetrahydrofuran (THF; dielectric constant $\epsilon = 7.4257$) was computed using density functional theory (DFT)¹¹ with Becke three-parameter exchange with the Perdew–Wang 1991 correlation (B3PW91).¹² Calculations of excitation energies and oscillator strengths in THF for the above optimized structures were performed by time-dependent (TD)-DFT with B3PW91. The LANL2DZ effective core potentials and valence basis set¹³ were used to describe the valence electrons of silver. Phosphorus, carbon, and hydrogen were described with 6-31+G*, 6-31G*, and 6-31G basis sets, respectively. Solvent effects were described by exploiting the integral equation formalism¹⁴ version of the polarizable continuum model,¹⁵ as implemented in Gaussian03¹⁶ and Gaussian09.¹⁷

A compact orbital representation for the electronic transition density matrix¹⁸ was calculated to interpret the qualitative nature of the T_1 state. The transition density matrix is given by $T_{ia} = \langle \phi_i | \hat{T} | \phi_a \rangle$, where ϕ_i and ϕ_a are occupied and virtual canonical MOs, respectively. The “natural transition orbitals” (NTOs) were obtained by orbital transformation followed by a singular value decomposition of the transition density matrix. In the NTO representation, the electronic transitions can be expressed by one single “electron–hole” pair with an associated eigenvalue of essentially 1, even transitions that are highly mixed in the canonical MO basis set. This procedure gives us a simple orbital interpretation of “what got excited to where”.¹⁹ All quantum-chemical calculations were carried out on a PC cluster system (Fujitsu). NTO calculations were performed using a laboratory-made code.

Synthesis of Compounds. 1,2-Bis[bis(2-methylphenyl)phosphino]benzene (L_{Me}). A THF solution of (2-methylphenyl)magnesium bromide (1 M, 25 mL, 25 mmol) was added dropwise to a solution of 1,2-bis(dichlorophosphino)benzene (1.0 g, 3.57 mol) in THF (20 mL) at 0 °C. The reaction mixture was stirred for 4 h at

room temperature, and then a solution of saturated aqueous NH_4Cl (100 mL) was added to the reaction mixture. The product was extracted with CH_2Cl_2 (3 \times 60 mL). The combined organic extracts were washed with saturated aqueous NaCl (150 mL) and dried over MgSO_4 . The drying agent was removed by filtration, and then the solvent was removed in vacuo to give a pale-yellow oil. The residue was purified by column chromatography on silica gel (*n*-hexane/ CH_2Cl_2 , 2:1) to afford L_{Me} (1.35 g, 75%) as a colorless solid. ^1H NMR (500 MHz, CD_2Cl_2 , 300 K): δ 2.19 (s, 12H), 6.76 (m, 4H), 6.92 (m, 2H), 7.02 (t, 4H, $J = 7.3$ Hz), 7.23–7.15 (m, 8H), 7.26 (m, 2H). ^{13}C NMR (125 MHz, CD_2Cl_2 , 300 K): δ 20.92 (t, $J(^{13}\text{C}-^{31}\text{P}) = 11.0$ Hz), 125.91, 128.52, 130.00, 133.61, 133.94, 135.44, 142.64 (t, $J(^{13}\text{C}-^{31}\text{P}) = 13.1$ Hz), 142.84 (t, $J(^{13}\text{C}-^{31}\text{P}) = 11.7$ Hz). $^{31}\text{P}\{^1\text{H}\}$ NMR (202 MHz, CD_2Cl_2 , 300 K): δ -27.10. Anal. Calcd for $\text{C}_{34}\text{H}_{32}\text{P}_2$: C, 81.26; H, 6.42; P, 12.33. Found: C, 80.99; H, 6.30; P, 12.18.

1,2-Bis[bis(2-ethylphenyl)phosphino]benzene (L_{Et}). A solution of (2-ethylphenyl)magnesium bromide in THF (25 mL) was prepared from magnesium (2.2 g, 90 mmol) and (2-bromoethyl)benzene (15.9 g, 86 mmol) and then cooled to 0 °C. A solution of 1,2-bis(dichlorophosphino)benzene (3.0 g, 10.1 mmol) in THF (20 mL) was added dropwise to the THF solution of (2-ethylphenyl)magnesium bromide. The reaction mixture was heated under reflux for 4 h. The mixture was cooled to room temperature. A solution of saturated aqueous NH_4Cl (150 mL) was added to the reaction mixture, and then the product was extracted with CH_2Cl_2 (3 \times 60 mL). The combined organic extracts were washed with saturated aqueous NaCl (150 mL) and dried over MgSO_4 . The drying agent was removed by filtration, and the solvent was removed in vacuo to give a pale-yellow oil. The residue was purified by column chromatography on silica gel (*n*-hexane/ CH_2Cl_2 , 2:1) to afford L_{Et} (2.15 g, 36%) as a colorless solid. ^1H NMR (500 MHz, CD_2Cl_2 , 300 K): δ 0.99 (t, 12H, $J = 7.5$ Hz), 2.60 (m, 8H), 6.79 (m, 4H), 6.91 (m, 2H), 7.02 (t, 4H, $J = 7.3$ Hz), 7.20–7.26 (m, 10H). ^{13}C NMR (125 MHz, CD_2Cl_2 , 300 K): δ 14.91, 27.51 (t, $J(^{13}\text{C}-^{31}\text{P}) = 11.3$ Hz), 125.81, 128.19 (t, $J(^{13}\text{C}-^{31}\text{P}) = 2.6$ Hz), 128.73, 129.08, 134.16, 134.43 (t, $J(^{13}\text{C}-^{31}\text{P}) = 3.1$ Hz), 135.56 (t, $J(^{13}\text{C}-^{31}\text{P}) = 3.3$ Hz), 143.74 (t, $J(^{13}\text{C}-^{31}\text{P}) = 12.0$ Hz), 148.69 (t, $J(^{13}\text{C}-^{31}\text{P}) = 12.8$ Hz). $^{31}\text{P}\{^1\text{H}\}$ NMR (202 MHz, CD_2Cl_2 , 300 K): δ -29.81. Anal. Calcd for $\text{C}_{38}\text{H}_{40}\text{P}_2$: C, 81.69; H, 7.22; P, 11.09. Found: C, 81.38; H, 6.89; P, 10.91.

1,2-Bis[bis(2-isopropylphenyl)phosphino]benzene (L_{IPr}). This compound was prepared using the same procedure as that of L_{Et} , except that (2-bromoisopropyl)benzene (17.1 g, 86 mmol) was used instead of (2-bromoethyl)benzene. Column chromatography on silica gel (*n*-hexane/ CH_2Cl_2 , 2:1) gave analytically pure L_{IPr} (805 mg, 12%) as a colorless solid. ^1H NMR (500 MHz, CD_2Cl_2 , 300 K): δ 0.90 (d, 12H, $J = 6.7$ Hz), 1.03 (br s, 12H), 3.34 (br s, 4H), 6.80 (m, 4H), 6.92 (m, 2H), 7.03 (t, 4H, $J = 7.3$ Hz), 7.23 (m, 2H), 7.30 (m, 8H). ^{13}C NMR (125 MHz, CD_2Cl_2 , 300 K): δ 23.19 (br), 23.85, 31.28 (t, $J(^{13}\text{C}-^{31}\text{P}) = 13.0$ Hz), 125.27 (t, $J(^{13}\text{C}-^{31}\text{P}) = 2.3$ Hz), 125.72, 128.86, 129.06, 134.21, 134.44 (t, $J(^{13}\text{C}-^{31}\text{P}) = 2.7$ Hz), 134.99, 144.46 (t, $J(^{13}\text{C}-^{31}\text{P}) = 12.3$ Hz), 153.35 (t, $J(^{13}\text{C}-^{31}\text{P}) = 12.3$ Hz). $^{31}\text{P}\{^1\text{H}\}$ NMR (202 MHz, CD_2Cl_2 , 300 K): δ -31.47. Anal. Calcd for $\text{C}_{42}\text{H}_{48}\text{P}_2$: C, 82.05; H, 7.87; P, 10.08. Found: C, 82.24; H, 7.69; P, 10.31.

$[\text{Ag}(\text{L})_2]\text{PF}_6$ (1). This compound was synthesized according to the literature.^{3a} ^1H NMR (500 MHz, CD_2Cl_2 , 300 K): δ 7.53 (m, 8H), 7.33 (m, 8H), 7.11–7.10 (m, 32H). ^1H NMR (500 MHz, CD_2Cl_2 , 220 K): δ 7.05 (br m, 32H), 7.28 (br m, 8H), 7.52 (m, 4H), 7.55 (m, 4H). ^{13}C NMR (125 MHz, CD_2Cl_2 , 220 K): δ 128.19, 129.64, 129.90 (m), 130.54, 132.66 (m), 133.32, 139.05 (m). $^{31}\text{P}\{^1\text{H}\}$ NMR (202 MHz, CD_2Cl_2 , 300 K): δ 0.81 (d, $^1J(^{31}\text{P}-^{109}\text{Ag}) = 264$ Hz, $^1J(^{31}\text{P}-^{107}\text{Ag}) = 229$ Hz). ESI-MS. Calcd for $\text{C}_{60}\text{H}_{48}\text{AgP}_4$: m/z 999.18. Found: m/z 999.2 ($[\text{M} - \text{PF}_6^-]$). Anal. Calcd for $\text{C}_{60}\text{H}_{48}\text{AgF}_6\text{P}_5$: C, 62.90; H, 4.22. Found: C, 62.76; H, 4.39.

$[\text{Ag}(\text{L})(\text{L}_{\text{Me}})]\text{BF}_4$ (2). Silver(I) tetrafluoroborate (39 mg, 0.20 mmol) was added to a solution of L_{Me} (100 mg, 0.20 mmol) in THF (15 mL). The mixture was stirred and heated under reflux. After 2 h, L (89 mg, 0.20 mmol) was added, and again the mixture was stirred and heated under reflux for 2 h. Upon cooling, an insoluble solid was removed from the reaction mixture by filtration, and then the solvent was

removed in vacuo. The residue was purified by recrystallization from THF to give colorless crystals $[\text{Ag}(\text{L})(\text{L}_{\text{Me}})]\text{BF}_4 \cdot 2\text{THF}$ (2·2THF). Yield: 199 mg, 82%. ^1H NMR (500 MHz, CD_2Cl_2 , 300 K): δ 1.88 (s, 12H), 6.71 (m, 8H), 6.77 (m, 6H), 6.88 (m, 2H), 7.11 (m, 4H), 7.16–7.26 (m, 8H), 7.28–7.44 (m, 8H), 7.49 (m, 2H), 7.54 (m, 4H), 7.60 (m, 2H). ^1H NMR (500 MHz, CD_2Cl_2 , 220 K): δ 1.60 (s, 6H), 1.76 (s, 6H), 6.60 (m, 8H), 6.66 (m, 4H), 6.79 (m, 2H), 6.81 (m, 2H), 7.03 (m, 4H), 7.18 (m, 6H), 7.21 (m, 2H), 7.24 (m, 2H), 7.30 (t, 2H, $J = 7.5$ Hz), 7.34 (m, 2H), 7.40 (t, 2H, $J = 7.5$ Hz), 7.44 (m, 2H), 7.50 (m, 2H), 7.54 (t, 2H, $J = 7.5$ Hz), 7.58 (m, 2H). ^{13}C NMR (125 MHz, CD_2Cl_2 , 220 K): δ 21.17 (t, $J(^{13}\text{C}-^{31}\text{P}) = 8.4$ Hz), 21.36 (m), 125.91, 126.21, 127.73 (t, $J(^{13}\text{C}-^{31}\text{P}) = 4.3$ Hz), 128.30 (t, $J(^{13}\text{C}-^{31}\text{P}) = 13.0$ Hz), 128.43, 129.12, 129.37 (t, $J(^{13}\text{C}-^{31}\text{P}) = 11.6$ Hz), 129.54, 129.57 (t, $J(^{13}\text{C}-^{31}\text{P}) = 12.4$ Hz), 129.79, 129.94, 130.57, 130.65, 130.87, 131.24, 131.43, 131.49, 131.55, 131.97 (t, $J(^{13}\text{C}-^{31}\text{P}) = 13.9$ Hz), 133.24 (t, $J(^{13}\text{C}-^{31}\text{P}) = 8.8$ Hz), 134.89, 137.12, 137.13 (t, $J(^{13}\text{C}-^{31}\text{P}) = 28.1$ Hz), 137.59 (t, $J(^{13}\text{C}-^{31}\text{P}) = 30.6$ Hz), 140.05 (t, $J(^{13}\text{C}-^{31}\text{P}) = 9.6$ Hz), 141.24 (t, $J(^{13}\text{C}-^{31}\text{P}) = 9.1$ Hz). $^{31}\text{P}\{^1\text{H}\}$ NMR (202 MHz, CD_2Cl_2 , 300 K): δ -12.76 (2dt, $^1J(^{31}\text{P}-^{107}\text{Ag}) = 231$ Hz, $^1J(^{31}\text{P}-^{109}\text{Ag}) = 268$ Hz, $^2J(^{31}\text{P}-^{31}\text{P}) = 23$ Hz), -2.86 (2dt, $^1J(^{31}\text{P}-^{107}\text{Ag}) = 227$ Hz, $^1J(^{31}\text{P}-^{109}\text{Ag}) = 262$ Hz, $^2J(^{31}\text{P}-^{31}\text{P}) = 31$ Hz). ESI-MS. Calcd for $\text{C}_{64}\text{H}_{56}\text{AgP}_4$: m/z 1055.24. Found: m/z 1055.2 ($[\text{M} - \text{BF}_4^-]$). Anal. Calcd for $\text{C}_{72}\text{H}_{72}\text{AgBF}_4\text{O}_2\text{P}_4$ (2·2THF): C, 67.15; H, 5.63. Found: C, 67.34; H, 5.58.

$[\text{Ag}(\text{L})(\text{L}_{\text{Et}})]\text{BF}_4$ (3). Silver(I) tetrafluoroborate (39 mg, 0.20 mmol) was added to a solution of L_{Et} (110 mg, 0.20 mmol) in THF (15 mL). The mixture was stirred and heated under reflux. After 2 h, L (89 mg, 0.20 mmol) was added, and then the mixture was again stirred and heated under reflux for 2 h. Upon cooling, an insoluble solid was removed from the reaction mixture by filtration, and then the solvent was removed in vacuo. The residue was purified by recrystallization from acetone to give colorless crystals $[\text{Ag}(\text{L})(\text{L}_{\text{Et}})]\text{BF}_4 \cdot (\text{CH}_3)_2\text{CO}$ (3·(CH₃)₂CO). Yield: 221 mg, 88%. ^1H NMR (500 MHz, CD_2Cl_2 , 300 K): δ 0.17 (t, 6H, $J = 7.3$ Hz), 0.38 (t, 6H, $J = 7.3$ Hz), 2.12 (dq, 2H, $J = 15.8$ and 7.8 Hz), 2.31 (m, 4H), 2.57 (dq, 2H, $J = 15.8$ and 7.8 Hz), 6.62 (m, 4H), 6.75 (m, 4H), 6.79 (m, 6H), 7.01 (m, 2H), 7.13–7.18 (m, 8H), 7.23 (t, 2H, $J = 7.5$ Hz), 7.24–7.29 (m, 4H), 7.38 (t, 2H, $J = 7.5$ Hz), 7.43 (m, 4H), 7.45 (m, 2H), 7.54 (m, 2H), 7.60 (m, 2H), 7.65 (t, 2H, $J = 7.5$ Hz). ^{13}C NMR (125 MHz, CD_2Cl_2 , 300 K): δ 10.99, 11.84, 27.52 (t, $J(^{13}\text{C}-^{31}\text{P}) = 9.6$ Hz), 27.75 (m), 126.49, 127.02, 128.19, 128.28, 128.84 (t, $J(^{13}\text{C}-^{31}\text{P}) = 4.4$ Hz), 129.25 (t, $J(^{13}\text{C}-^{31}\text{P}) = 4.7$ Hz), 130.17, 130.23 (t, $J(^{13}\text{C}-^{31}\text{P}) = 10.5$ Hz), 130.48, 130.62, 130.76 (t, $J(^{13}\text{C}-^{31}\text{P}) = 17.3$ Hz), 130.90, 131.32, 131.43 (t, $J(^{13}\text{C}-^{31}\text{P}) = 13.2$ Hz), 134.88, 131.96, 132.43, 132.82 (t, $J(^{13}\text{C}-^{31}\text{P}) = 8.1$ Hz), 132.88 (t, $J(^{13}\text{C}-^{31}\text{P}) = 8.7$ Hz), 133.76 (t, $J(^{13}\text{C}-^{31}\text{P}) = 8.7$ Hz), 135.80, 138.29, 138.92 (t, $J(^{13}\text{C}-^{31}\text{P}) = 26.4$ Hz), 139.17 (t, $J(^{13}\text{C}-^{31}\text{P}) = 25.1$ Hz), 146.02 (t, $J(^{13}\text{C}-^{31}\text{P}) = 9.1$ Hz), 146.90 (t, $J(^{13}\text{C}-^{31}\text{P}) = 8.7$ Hz). $^{31}\text{P}\{^1\text{H}\}$ NMR (202 MHz, CD_2Cl_2 , 300 K): δ -15.16 (2dt, $^1J(^{31}\text{P}-^{109}\text{Ag}) = 267$ Hz, $^1J(^{31}\text{P}-^{107}\text{Ag}) = 233$ Hz, $^2J(^{31}\text{P}-^{31}\text{P}) = 31$ Hz), -4.25 (2dt, $^1J(^{31}\text{P}-^{109}\text{Ag}) = 263$ Hz, $^1J(^{31}\text{P}-^{107}\text{Ag}) = 228$ Hz, $^2J(^{31}\text{P}-^{31}\text{P}) = 31$ Hz). ESI-MS. Calcd for $\text{C}_{68}\text{H}_{64}\text{AgP}_4$: m/z 1111.30. Found: m/z 1111.3 ($[\text{M} - \text{BF}_4^-]$). Anal. Calcd for $\text{C}_{68}\text{H}_{64}\text{AgBF}_4\text{P}_4$: C, 68.07; H, 5.38. Found: C, 67.82; H, 5.21.

RESULTS AND DISCUSSION

Synthesis and Characterization of dppb Derivatives and Heteroleptic Silver(I) Complexes. Bidentate bisphosphine ligands were synthesized from bis(dichlorophosphino)benzene and the appropriate Grignard reagents: (2-methylphenyl)magnesium bromide for L_{Me} , (2-ethylphenyl)magnesium bromide for L_{Et} , and (2-isopropylphenyl)magnesium bromide for L_{IPr} .²⁰ Large alkyl substituents at the ortho position of the peripheral phenyl groups of dppb considerably decreased the yield of the derivative because of their steric encumbrances; the yields were 75% for L_{Me} , 36% for L_{Et} and 12% for L_{IPr} . Heteroleptic complex **2** was prepared by heating **1** equiv of L_{Me} and **1** equiv of AgPF_6 under reflux in THF under a

dinitrogen atmosphere with stirring. After reaction for 2 h, the solid silver salt completely dissolved and the solution became clear, presumably because of the formation of $\text{Ag}(\text{L}_{\text{Me}})(\text{THF})_n$ ($n = 1$ or 2). A total of 1 equiv of L was then added, and the solution was heated under reflux for a further 2 h. The reaction mixture was filtered, and then the solvent was removed in vacuo to give the crude heteroleptic complex. Recrystallization from THF was sufficient to purify **2** by removing a small amount of the homoleptic byproduct $[\text{Ag}(\text{L})_2]\text{BF}_4$. Complex **3** was prepared in a manner similar to **2**, except that **3** was recrystallized from acetone. High yields of 82% and 88% were obtained for **2** and **3**, respectively.

We were unable to synthesize $[\text{Ag}(\text{L}_{\text{iPr}})(\text{L})]\text{BF}_4$ using L_{iPr} under the reaction conditions described above. The isolated product was solely a stoichiometric amount of homoleptic $[\text{Ag}(\text{L})_2]\text{BF}_4$, suggesting that heteroleptic $[\text{Ag}(\text{L}_{\text{iPr}})(\text{L})]\text{BF}_4$, if produced, readily undergoes disproportionation to yield the homoleptic complex. It is concluded that the bulkiness of the alkyl group at the ortho position of the phenyl groups in the dppb derivatives governs the stability of the resulting heteroleptic complexes; the more bulky the alkyl group, the less stable the heteroleptic complex. Furthermore, attempts to prepare homoleptic complexes $[\text{Ag}(\text{L}_{\text{R}})_2]\text{BF}_4$ ($\text{R} = \text{Me}, \text{Et},$ and iPr) only generate mono-diphosphine silver(I) complexes.

The crystal structures of complexes **1–3** are shown in Figure 1a–c. Selected bond lengths and angles are summarized in Table 1. The *o*-methyl and *o*-ethyl groups are oriented in the direction of the central metal, resulting in interligand steric interactions between the four peripheral phenyl groups of the other ligand (L) in solution. The coordination geometries of **1–3** are distorted from a D_{2d} pseudotetrahedral geometry that

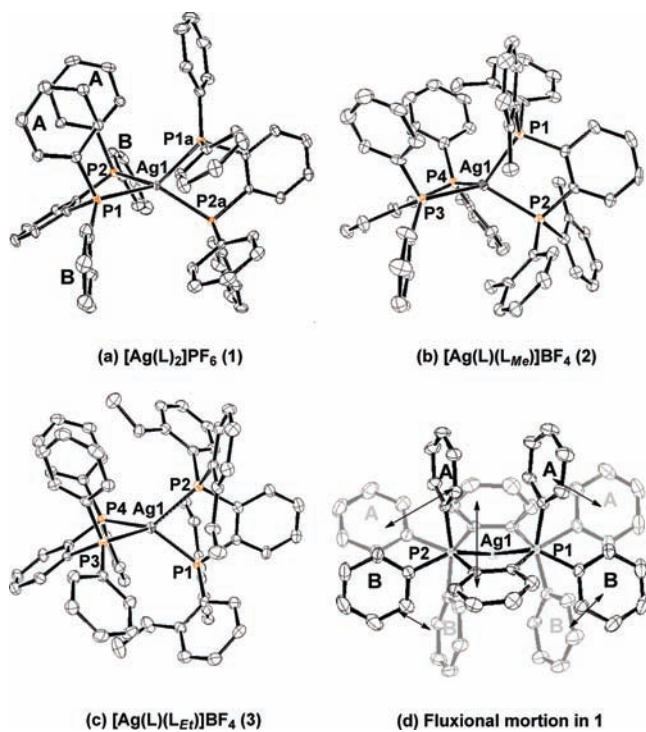


Figure 1. ORTEP drawings of the structures of cations in **1** (a), **2** (b), and **3** (c). Thermal ellipsoids are drawn at the 50% probability level. Hydrogen atoms and counteranions PF_6^- and BF_4^- are omitted for clarity. The two types of phenyl groups (A and B) and fluxional motion in **1** are shown in parts a and d, respectively.

Table 1. Selected Bond Distances (Å) and Angles (deg) for **1–3**

	1 ^c		2	3
Ag–P1 ^a	2.4592(6)	2.5435(6)	2.553(2)	2.5147(10)
Ag–P2 ^a	2.5027(6)	2.4611(6)	2.4958(19)	2.5063(10)
Ag–P3			2.501(2)	2.5030(10)
Ag–P4			2.519(2)	2.5216(10)
average (Ag–P)	2.492		2.517	2.511
dihedral angle ^b	82.56(3)	85.25(3)	84.91(10)	81.38(4)

^aP1 and P2 belong to L for **1**, L_{Me} for **2**, and L_{Et} for **3**. ^bThe dihedral angle between two planes, P1–Ag–P2 and P3(1a)–Ag–P4(2a). ^cTwo molecules in the unit cell.

might be expected for a d^{10} ion. The dihedral angles between the two planes defined by P1–Ag^I–P2 and P3(1a)–Ag^I–P4(2a) are 81.38(4)–85.25(3)°. The average bond lengths (Ag–P) in **2** and **3** are almost equal to those in **1**, suggesting that the chelating abilities of L_{Me} and L_{Et} are similar to that of L .

The strong chelating abilities of the dppb derivatives were confirmed by $^{31}\text{P}\{^1\text{H}\}$ NMR spectroscopic measurements in CD_2Cl_2 . It is known that Ag–P coupling in the room temperature spectra of silver phosphine complexes is unresolved because of the rapid exchange equilibria.²¹ Complexes **1–3**, however, show typical Ag–P couplings even at ambient temperature. Complex **1** shows two doublet of doublets with $J(^{31}\text{P}–^{107}\text{Ag}) = 229$ Hz and $J(^{31}\text{P}–^{109}\text{Ag}) = 264$ Hz, and **2** and **3** exhibit two doublet of triplets (A_2X_2 systems). As an example, the $^{31}\text{P}\{^1\text{H}\}$ NMR spectrum of **3** is shown in Figure 2. Two well-resolved pairs of doublet of triplets are

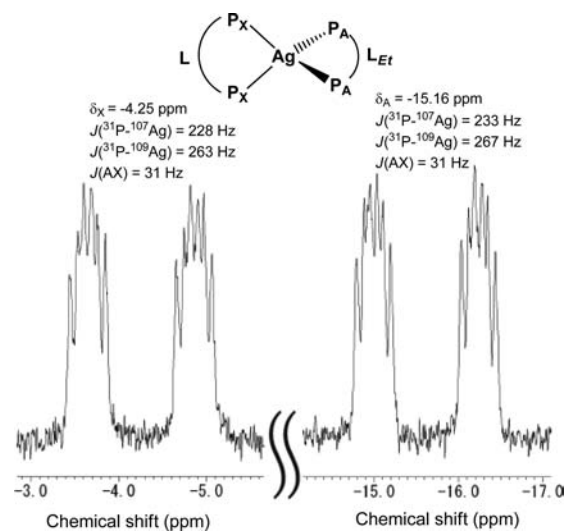


Figure 2. $^{31}\text{P}\{^1\text{H}\}$ NMR spectrum of **3** (in CD_2Cl_2 at 300 K).

observed at -15.16 and -4.25 ppm with $^2J(\text{AX}) = 31/{}^1J(^{31}\text{P}–^{107}\text{Ag}) = 233/{}^1J(^{31}\text{P}–^{109}\text{Ag}) = 267$ Hz and $^2J(\text{AX}) = 31/{}^1J(^{31}\text{P}–^{107}\text{Ag}) = 228/{}^1J(^{31}\text{P}–^{109}\text{Ag}) = 263$ Hz, respectively. Because no signals from disproportionation products were observed, the heteroleptic structures of **2** and **3** are concluded to be very stable even in solution. Furthermore, ^1H NMR experiments revealed that **3** has the most rigid structure in solution. The ring protons of the two types of phenyl groups (labeled as A and B in Figure 1a)

bonded to the phosphorus atom in 1–3 are nonequivalent because of the weak π – π interaction between two type A phenyl groups. However, the ^1H NMR spectra of 1 in CD_2Cl_2 at 300 and 220 K show ring protons of A and B as a single broad peak (see Figure S8 in the SI). This can be attributed to rapid interconversion based on a dynamic fluxional process in 1 (Figure 1d). In the case of 2 at 220 K, the protons attached to phenyl and tolyl groups are observed as four kinds of well-resolved signals consistent with aryl groups, and the methyl protons of L_{Me} appear as two sharp singlets (see Figure S9 in the SI). These two singlets become one broad singlet at 300 K in CD_2Cl_2 (see Figure S10 in the SI). However, the four multiplets observed for the two kinds of tolyl and phenyl groups are still observed at 300 K (see Figure S8 in the SI), suggesting there is no fluxional motion of 2 at either 220 or 300 K. A possible explanation for this is that a small waving motion of the two diphosphine ligands in 2 makes the methyl protons of L_{Me} chemically equivalent at 300 K. In contrast, the ^1H NMR spectrum of 3 exhibits two sharp triplets [$\text{CH}_3(\text{A})$, 0.17 ppm; $\text{CH}_3(\text{B})$, 0.38 ppm] corresponding to the terminal methyl protons of L_{Et} (Figure 3). Moreover, the methylene protons of

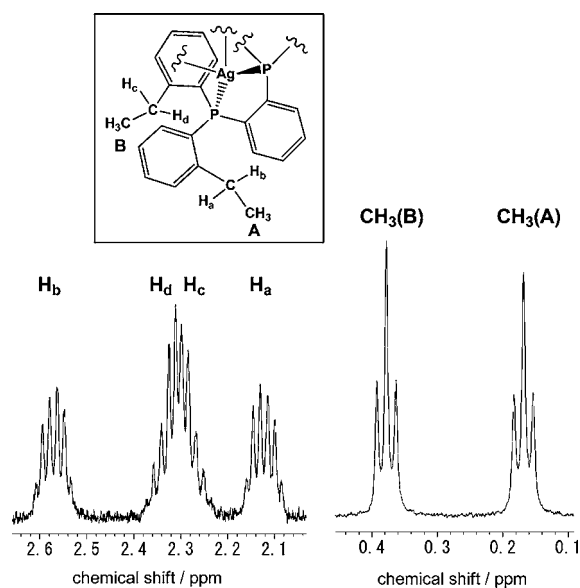


Figure 3. ^1H NMR spectrum of 3 (in CD_2Cl_2 at 300 K).

the ethyl substituents are split into two doublet of quartets and one multiplet consisting of two doublet of quartets (H_a – d) with $J = 7.8$ and 15.8 Hz in CD_2Cl_2 at 300 K. Resonance signals (H_a , 2.12 ppm; H_b , 2.57 ppm; H_c , 2.29 ppm; H_d , 2.32 ppm) were assigned using COSY ^1H NMR spectra. These results demonstrate that complex 3 does not exhibit fluxional motion or rotation about the C_{aryl} – $\text{C}_{\text{ethylene}}$ bonds. Similarly, the motion of the P – C_{aryl} bonds in 3 is obstructed in solution at ambient temperature on the NMR time scale. The NMR studies of 1–3 lead to the conclusion that interligand steric interactions fix the geometry of 3 in solution.

Photophysical Properties of dppb Derivatives. dppb derivatives have two types of aromatic groups attached to phosphorus atoms; a bridging *o*-phenylene group and four peripheral phenyl groups (phenyl for **L**, methylphenyl for L_{Me} , ethylphenyl for L_{Et} and isopropyl for L_{iPr}). The absorption and phosphorescence spectra of the diphosphine ligands in 2-MeTHF at 77 K are shown in Figure 4, and their photophysical

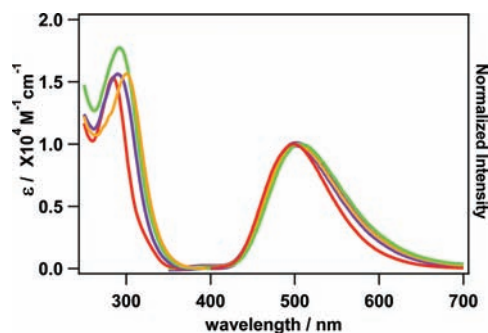


Figure 4. Absorption and corrected emission spectra of **L** (red), L_{Me} (purple), L_{Et} (green), and L_{iPr} (orange) in 2-MeTHF at 77 K; $\lambda_{\text{exc}} = 300$ nm.

properties are summarized in Table 2. These diphosphine ligands exhibit quite similar behavior; the absorption spectra

Table 2. Photophysical Data for Diphosphine Ligands in 2-MeTHF

ligand	absorption $\lambda_{\text{max}}/\text{nm}$ ($\epsilon/\text{M}^{-1}\text{cm}^{-1}$) ^a	emission $\lambda_{\text{max}}/\text{nm}$ ^a	Φ_{PL} ^b	E_{pa} (V) vs Fc/ Fc^+ ^c
L	284 (1.51×10^4)	499	0.68	+0.36
L_{Me}	290 (1.53×10^4)	500	0.75	+0.40
L_{Et}	292 (1.73×10^4)	505	0.70	+0.44
L_{iPr}	300 (1.58×10^4)	500	0.69	+0.38

^aAbsorption and PL peak wavelength in 2-MeTHF at 77 K; $\lambda_{\text{exc}} = 300$ nm. ^bAbsolute PL quantum yield in 2-MeTHF at 77 K; $\lambda_{\text{exc}} = 300$ nm. ^cAnodic peak potential in argon-saturated CH_3CN at 293 K. These waves are irreversible.

display broad, intense bands at 284–300 nm [extinction coefficient (ϵ) = $\sim 16000 \text{ M}^{-1} \text{ cm}^{-1}$], which are characteristic of arylphosphine compounds, as shown in Figure 4.²² These bands are assigned to a mixed transition of $1-\pi^*$ and $\pi-\pi^*$; the former is the transition of an electron from the lone-pair orbital on phosphorus to an empty antibonding π orbital on an *o*-phenylene or phenyl-type ring, while the latter are transitions localized on a phenyl-type or phenylene ring and those from a phenyl-type ring to a phenylene ring. These assignments are consistent with recent MO calculations on dppb.²³ Solutions of all of these diphosphine ligands are not emissive at room temperature, but strong blue-green emission ($\lambda_{\text{max}} = 499$ –505 nm; $\Phi_{\text{p}} = 0.68$ –0.75) is observed in frozen 2-MeTHF at 77 K (Figure 4). Our calculations revealed that the emitting state of dppb is mainly the charge-transfer state from the lone pair on the phosphorus atoms to the *o*-phenylene groups.⁹ The dppb derivatives exhibit absorption and phosphorescence spectra quite similar to those of dppb, suggesting that alkyl substituents (methyl, ethyl, and isopropyl) at ortho positions in peripheral aryl rings have a small effect on the electronic states of these ligands.

The electrochemical properties of the diphosphine ligands were investigated by cyclic voltammetry (CV). The oxidation potentials of diphosphine ligands (**L**, L_{Me} , L_{Et} and L_{iPr}) are very similar to each other, as shown in Table 2.

Photophysical Properties of Silver(I) Complexes 1–3 in 2-MeTHF Glasses at 77 K and a Comparison with MO Calculations. Figure 5 shows the absorption and emission spectra of silver(I) complexes 1–3 at 77 K in 2-MeTHF. Absorption and emission peaks, lifetimes (τ_{T}), Φ_{p} at 77 K, and DFT calculation data (dihedral angles and T_1 energy levels) are

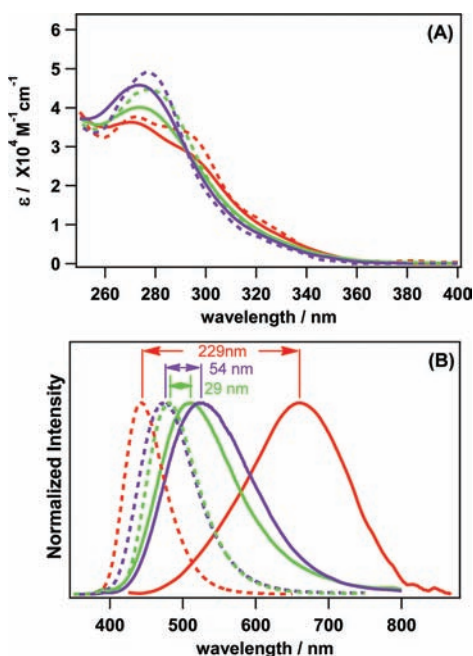


Figure 5. (A) Absorption and (B) corrected emission spectra for **1** (red), **2** (purple), and **3** (green) in 2-MeTHF at 77 K (dashed lines) and 293 K (solid lines); $\lambda_{\text{exc}} = 300$ nm.

summarized in Table 3. The optimized S_0 structures in THF were used for these calculations. Complexes **1–3** show

Table 3. Photophysical Data for Complexes 1–3 in 2-MeTHF at 77 K

complex	absorption $\lambda_{\text{max}}/\text{nm}$ ($\epsilon/M^{-1}\text{cm}^{-1}$) ^a	$\lambda_{\text{max}}/\text{nm}$ (τ/ms) ^a	Φ_{PL} ^b	dihedral angle/deg ^c	T_1/nm^c
1	272 (3.77×10^4)	441 (2.3)	0.88	81	360
2	276 (4.01×10^4)	473 (2.5)	0.75	78	365
3	278 (4.46×10^4)	480 (2.8)	0.70	77	365

^aAbsorption and PL peak wavelength in 2-MeTHF at 77 K; $\lambda_{\text{exc}} = 300$ nm. ^bAbsolute PL quantum yield in 2-MeTHF at 77 K; $\lambda_{\text{exc}} = 300$ nm. ^cDihedral angle between two planes, P1–Ag–P2 and P3(1a)–Ag–P4(2a), and the $T_1 \leftarrow S_0$ energy were calculated for the optimized S_0 structures of **1–3**.

absorption spectra typical of diphosphine ligands; broad bands with maxima at 272–278 nm are assigned to a mixed transition of $\sigma \rightarrow \pi^*$ and $\pi-\pi^*$. Complexes **1–3** show efficient luminescence performance at 77 K, as listed in Table 3. Strong blue phosphorescence from **1–3** was observed in frozen 2-MeTHF ($\lambda_{\text{max}} = 441\text{--}480$ nm; $\Phi_{\text{p}} = 0.70\text{--}0.88$). Because a change of the structure of the excited state is highly restricted in 2-MeTHF glass at 77 K because of the rigidity of the medium, blue phosphorescence is concluded to arise from an excited state with a tetrahedral structure.

The MO calculations determined the dihedral angles between the two planes P1–Ag–P2 and P3(1a)–Ag–P4(2a) for **1–3** in a THF solution to be 81, 78, and 77°, respectively, which are smaller than those found in X-ray crystal structures. This can be attributed to the presence of a BF_4^- counteranion, trapped solvent in the crystal lattice, and weak noncovalent interactions ($\pi-\pi$, hydrogen-bonding, and CH– π interactions) in single crystals.

NTO analyses were performed to clarify the origin of phosphorescence in the complexes. Maps of the hole

[approximately the highest occupied molecular orbitals (HOMO)] and electron [approximately the lowest unoccupied molecular orbital (LUMO)] in T_1 in the optimized S_0 structure of **3** are shown in Figure 6. The hole distribution in **3** is mainly

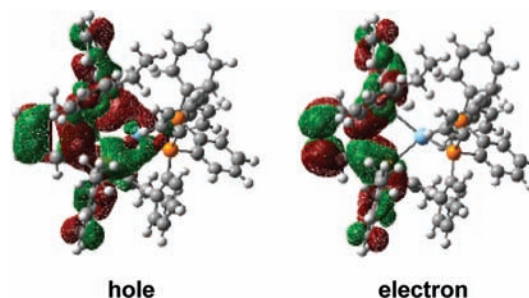


Figure 6. NTO pairs for the lowest triplet excited state of **3** in the optimized S_0 geometry. The generation probability is 56%.

confined to the orbitals of the σ bonds between the silver(I) and two phosphorus (L_{Et}) atoms and slightly extended over the π system of L_{Et} ; the contributions from the silver, phosphorus, and other (π) systems are 4, 22, and 74%, respectively (see Table S2 in the SI). The electron distribution is essentially delocalized over L_{Et} . These results indicate that strong blue phosphorescence mainly results from $\pi-\pi^*$ transitions (the contribution is about 81%), which include transitions localized on a phenyl group and a phenylene ring as well as those with charge-transfer character from a phenyl-type ring to a phenylene ring. The long lifetimes (2.3–2.8 ms) of **1–3** at 77 K support the assignment of the origin of phosphorescence as $\pi-\pi^*$. Meanwhile, the contribution from the $\sigma-\pi^*$ transition to phosphorescence is 19%. The $\sigma-\pi^*$ transition contains contributions from MLCT (4%) and intraligand charge-transfer (ILCT, 15%) transitions because the σ orbital is primarily composed of d orbitals (silver atom; d_{xy} , d_{yz} , d_{zx}) and p orbitals (phosphorus atoms) including lone-pair electrons. Complexes **1** and **2** show similar NTO maps (see Figures S17 and S18 in the SI) and origin of phosphorescence to **3** (see Tables S3 and S4 in the SI); the contribution from $\pi-\pi^*$ is 78% for **1** and 82% for **2**.

Molecular motion in 2-MeTHF at 77 K is strongly prohibited in both the ground and excited states because of the high viscosity of the medium. Thus, the structures of complexes **1–3** resemble the optimized S_0 with pseudotetrahedral geometry even in the T_1 state. λ_{max} is located at 441 nm for **1**, 473 nm for **2**, and 480 nm for **3**. From Table 3, it is obvious that λ_{max} shifts to longer wavelength as the dihedral angle of the optimized S_0 structure of the complex decreases.

Photophysical Properties of Silver Complexes 1–3 at Room Temperature. Figure 5 shows the absorption and emission spectra of silver complexes **1–3** at 293 K in 2-MeTHF. Photophysical and calculated data are summarized in Table 4. The optimized T_1 structures in THF were used for these calculations. Complex **1** exhibits bright blue emission in 2-MeTHF glasses, whereas it shows weak orange luminescence ($\lambda_{\text{max}} = 670$ nm; $\Phi_{\text{p}} = 0.05$) in degassed 2-MeTHF at room temperature (red dashed and solid lines in Figure 5B). Although the MLCT character responsible for the Jahn–Teller effect is not strong (4% for **1**), the large red shift of the emission peak of 230 nm and the low Φ_{p} in 2-MeTHF at room temperature indicate that a large change in the geometry of **1** occurs in the excited state from pseudotetrahedral to a more

Table 4. Photophysical Data for Complexes 1–3 in 2-MeTHF at 293 K

complex	absorption λ_{\max}/nm ($\epsilon/M^{-1}\text{cm}^{-1}$) ^a	λ_{\max}/nm ($\tau/\mu\text{s}$) ^a	Φ_{PL} ^b	dihedral angle/deg ($\Delta\theta^d/\text{deg}$) ^c	T_1/nm^c	$E_{1/2}/V^e$ ($\Delta E_p/\text{mV}$) ^f
1	270 (3.63×10^4)	670 (22)	0.05	30 (51)	612	+0.48 (80)
2	274 (4.58×10^4)	527 (10)	0.33	65 (13)	596	+0.70 (80)
3	274 (4.01×10^4)	509 (15)	0.26	70 (7)	526	+0.72 (130)

^aAbsorption and PL peak wavelength in 2-MeTHF at 77 K; $\lambda_{\text{exc}} = 300$ nm. ^bAbsolute PL quantum yield in 2-MeTHF at 77 K; $\lambda_{\text{exc}} = 300$ nm. ^cDihedral angle between two planes, P1–Ag–P2 and P3(1a)–Ag–P4(2a), and $T_1 \leftarrow S_0$ energy were calculated for the optimized T_1 structures of 1–3. ^dDifference in dihedral angles between optimized S_0 and T_1 structures. ^eHalf-wave potential (vs Fc/Fc⁺) recorded in argon-saturated CH₃CN. ^fPeak-to-peak separation.

flattened structure, which is accompanied by energetic relaxation. The calculated dihedral angle (30°) and T_1 energy (612 nm) of **1** in the optimized T_1 structure also suggest that the structure of the excited state is flatter; the angular difference from the optimized S_0 structure is as large as 51° (Table 4).

Complexes **2** and **3** exhibit intense green phosphorescence ($\Phi_p = 0.33$ and 0.26) in a 2-MeTHF solution at 293 K (purple lines for **2** and green for **3** in Figure 5B). The phosphorescence peaks are located at longer wavelengths than those at 77 K. However, the shifts are smaller: 54 nm for **2** and 29 nm for **3**. Therefore, the excited states of **2** and **3** undergo some changes in geometry at room temperature, resulting in a small energetic relaxation of the phosphorescent state.

The emitting state in solution at 293 K is considered to have the optimized T_1 structure. The MO calculations revealed that the calculated dihedral angles between two planes, P1–Ag–P2 and P3(1a)–Ag–P4(2a), in the optimized T_1 structures are 65° for **2** and 70° for **3**. These angles are at most 13° smaller than those in the optimized S_0 structures. The interligand steric interactions caused by alkyl substituents at the ortho positions in L_{Me} and L_{Et} probably prevent adoption of a flattened geometry.

A single reversible wave was observed for silver complexes **1**–**3** by CV at $E_{1/2} = +0.48$, +0.70, and +0.72V vs Fc/Fc⁺ in CH₃CN, respectively (Table 4). Silver(I) in **1** is oxidized more readily than that in **2** and **3**. This result is consistent with the fact that interligand steric interactions stabilize the tetrahedral silver(I) versus flattened silver(II) complexes in **2** and **3** in solution at 293 K. A similar correlation between the degree of steric effects and the one-electron-oxidation potential was reported for tetrahedral copper(I) diimine complexes.²⁴

NTO analysis based on the optimized T_1 structure in THF showed that transitions can be described as single-electron pairs, which reproduce over 90% of the transition density. The maps from NTO analysis based on the optimized T_1 structure of **3** in THF are shown in Figure 7 as an example. It is clear that the hole distribution of **3** mainly lies on σ orbitals composed of

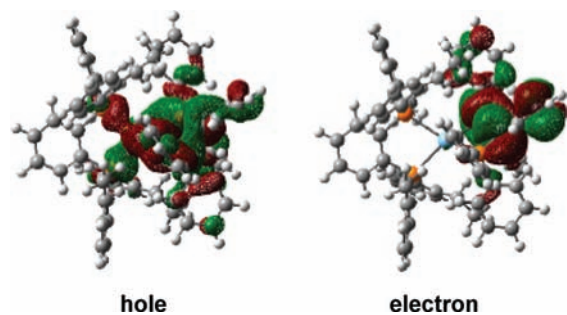


Figure 7. NTO pairs for the lowest triplet excited state of **3** in the optimized T_1 geometry. The generation probability is 90%.

silver and four phosphorus atoms, and the distribution on the π system appreciably decreases compared to that of **3** in the optimized S_0 structure, as seen in Figure 6. The electron distribution is largely confined to the *o*-phenylene group. Thus, the contribution of $\pi-\pi^*$ in phosphorescence decreases from 81% to 47%, and that of $\sigma-\pi^*$ increases to 53%; attributable fractions of MLCT and ILCT are 10% and 43%, respectively (see Table S5 in the SI). It is noteworthy that a small distortion (difference of the dihedral angle is 7°) between the optimized S_0 and T_1 structures in the excited state of **3** considerably alters the origin of phosphorescence. The distortion increases the hole energy levels by reducing the symmetry (from D_{2d}), which removes the degeneracy of the HOMO energy levels. If the hole energy levels increase, the contribution of π orbitals in diphosphine ligands to the hole decreases, so the $\pi-\pi^*$ character of phosphorescence is reduced.

When the contribution of the d orbitals in the silver atom and p orbitals in phosphorus atoms to the hole increases, the $\sigma-\pi^*$ character of phosphorescence increases. Complex **2** possesses NTO maps similar to those of **3** (see Figure S19 in the SI), while details of the origin of phosphorescence are shown in Table S6 in the SI. The contributions of $\sigma-\pi^*$ and $\pi-\pi^*$ transitions are 52% and 48%, respectively, for **2**.

CONCLUSIONS

The synthesis and photophysics of heteroleptic tetrahedral silver(I) complexes **2** and **3** containing diphosphine ligands have been reported. ¹H and ³¹P{¹H} NMR experiments confirmed that the stability of heteroleptic silver(I) complexes **2** and **3** in solution and the alkyl substituents at the ortho positions of phenyl groups bonded to phosphorus atoms in diphosphine ligands induce a rigid environment around the silver center in **2** and **3**. Interligand steric interactions between the alkyl groups inhibit geometric relaxation of the excited state, leading to intense green phosphorescence from **2** and **3** in solution even at ambient temperature. The quantum yields of phosphorescence for **2** and **3** at 293 K are 0.33 and 0.26, which are ca. 6 times as large as that of the homoleptic complex **1**. On the basis of theoretical studies, the origin of green phosphorescence from the complexes **1**–**3** is ascribed to a mixture of $\sigma-\pi^*$ and $\pi-\pi^*$ transitions.

We believe that the introduction of *o*-alkyl substituents onto the phenyl groups of dppb ligands is an effective way to induce interligand steric interactions in metal complexes. Interligand steric interactions are expected to improve the luminescence of metal complexes in both solid crystals and solution.

ASSOCIATED CONTENT

Supporting Information

X-ray crystallographic data for complexes **2** and **3** in CIF format, X-ray crystallographic data of complexes **1**–**3**, NMR spectra and cyclic voltammograms of ligands and complexes **1**–

3, NTO pairs for the T_1 state, compositions of the hole and electron in the T_1 state, and geometry data for the optimized structures of 1–3. This material is available free of charge via the Internet at <http://pubs.acs.org>.

AUTHOR INFORMATION

Corresponding Author

*E-mail: osawa@postman.riken.jp

Notes

The authors declare no competing financial interest.

ACKNOWLEDGMENTS

The authors thank Dr. Daisuke Hashizume for technical assistance with X-ray structural analysis.

REFERENCES

- (1) (a) Yam, V. W. W.; Lo, K. K. W. *Mol. Supramol. Photochem.* **1999**, *4*, 31–112. (b) Che, C.-M.; Lai, S.-W. *Coord. Chem. Rev.* **2005**, *249*, 1296–1309. (c) Barbieri, A.; Accorsi, G.; Armaroli, N. *Chem. Commun.* **2008**, 2185–2193. (d) Yam, V. W.-W.; Wong, K. M.-C. *Chem. Commun.* **2011**, 47, 11579–11592.
- (2) (a) Jansen, M. *Angew. Chem.* **1987**, *99*, 1136–1149. (b) Bardaji, M.; Laguna, A. *Eur. J. Inorg. Chem.* **2003**, 3069–3079. (c) Catalano, V. J.; Bennett, B. L.; Malwitz, M. A.; Yson, R. L.; Kar, H. M.; Muratidis, S.; Horner, S. J. *Comments Inorg. Chem.* **2003**, *24*, 39–68. (d) Sculfort, S.; Braunstein, P. *Chem. Soc. Rev.* **2011**, *40*, 2741–2760.
- (3) (a) Osawa, M.; Hoshino, M. *Chem. Commun.* **2008**, 6384–6386. (b) Li, Y.-X.; Chen, Z.-F.; Xiong, R.-G.; Xue, Z.; Ju, H.-X.; You, X.-Z. *Inorg. Chem. Commun.* **2003**, *6*, 819–822. (c) Omary, M. A.; Rawashdeh-Omary, M. A.; Diyabalanage, H. V. K.; Dias, H. V. R. *Inorg. Chem.* **2003**, *42*, 8612–8614. (d) Wei, Y.-Q.; Wu, K.-C.; Zhuang, B.-T.; Zhou, Z.-F. *J. Mol. Struct.* **2005**, *751*, 133–138. (e) Kunkely, H.; Vogler, A. *Inorg. Chim. Acta* **2006**, *359*, 388–390. (f) Kunkely, H.; Vogler, A. *Inorg. Chem. Commun.* **2006**, *9*, 866–868. (g) Li, F.-F.; Ma, J.-F.; Yang, J.; Jia, H.-Q.; Hu, N.-H. *J. Mol. Struct.* **2006**, *787*, 106–112. (h) Belicchi Ferrari, M.; Bisceglie, F.; Cavalli, E.; Pelosi, G.; Tarasconi, P.; Verdolino, V. *Inorg. Chim. Acta* **2007**, *360*, 3233–3240. (i) Kunkely, H.; Vogler, A. *Inorg. Chem. Commun.* **2007**, *10*, 784–786. (j) Kunkely, H.; Vogler, A. *Inorg. Chem. Commun.* **2007**, *10*, 226–228. (k) Teets, T. S.; Partyka, D. V.; Esswein, A. J.; Updegraff, J. B., III; Zeller, M.; Hunter, A. D.; Gray, T. G. *Inorg. Chem.* **2007**, *46*, 6218–6220. (l) Kunkely, H.; Pawlowski, V.; Strasser, A.; Vogler, A. *Inorg. Chem. Commun.* **2008**, *11*, 415–417. (m) Matsumoto, K.; Shindo, T.; Mukasa, N.; Tsukuda, T.; Tsubomura, T. *Inorg. Chem.* **2010**, *49*, 805–814. (n) Tsukuda, T.; Kawase, M.; Dairiki, A.; Matsumoto, K.; Tsubomura, T. *Chem. Commun.* **2010**, *46*, 1905–1907. (o) Christofididis, G.; Cox, P. J.; Aslanidis, P. *Polyhedron* **2012**, *31*, 502–505.
- (4) (a) Wrighton, M.; Morse, D. L. *J. Am. Chem. Soc.* **1974**, *96*, 998–1003. (b) Watts, R. J.; Missimer, D. *J. Am. Chem. Soc.* **1978**, *100*, 5350–5357. (c) Zuleta, J. A.; Bevilacqua, J. M.; Rehm, J. M.; Eisenberg, R. *Inorg. Chem.* **1992**, *31*, 1332–1337. (d) Barakat, K. A.; Cundari, T. R.; Omary, M. A. *J. Am. Chem. Soc.* **2003**, *125*, 14228–14229. (e) Sinha, P.; Wilson, A. K.; Omary, M. A. *J. Am. Chem. Soc.* **2005**, *127*, 12488–12489.
- (5) (a) Everly, R. M.; Ziessel, R.; Suffert, J.; McMillin, D. R. *Inorg. Chem.* **1991**, *30*, 559–561. (b) Tran, D.; Bourassa, J. L.; Ford, P. C. *Inorg. Chem.* **1997**, *36*, 439–442. (c) Zhang, Q.; Zhou, Q.; Cheng, Y.; Wang, L.; Ma, D.; Jing, X.; Wang, F. *Adv. Mater.* **2004**, *16*, 432–436. (d) Zhang, Q.; Ding, J.; Cheng, Y.; Wang, L.; Xie, Z.; Jing, X.; Wang, F. *Adv. Funct. Mater.* **2007**, *17*, 2983–2990. (e) Smith, C. S.; Branham, C. W.; Marquardt, B. J.; Mann, K. R. *J. Am. Chem. Soc.* **2010**, *132*, 14079–14085. (f) Czerwieńiec, R.; Yu, J.-B.; Yersin, H. *Inorg. Chem.* **2011**, *50*, 8293–8301.
- (6) (a) McMillin, D. R.; McNett, K. M. *Chem. Rev.* **1998**, *98*, 1201–1219. (b) Ford, P. C.; Cariati, E.; Bourassa, J. *Chem. Rev.* **1999**, *99*, 3625–3647. (c) Felder, D.; Nierengarten, J.-F.; Barigelletti, F.; Ventura, B.; Armaroli, N. *J. Am. Chem. Soc.* **2001**, *123*, 6291–6299. (d) Cuttell, D. G.; Kuang, S.-M.; Fanwick, P. E.; McMillin, D. R.; Walton, R. A. *J. Am. Chem. Soc.* **2002**, *124*, 6–7. (e) Kuang, S.-M.; Cuttell, D. G.; McMillin, D. R.; Fanwick, P. E.; Walton, R. A. *Inorg. Chem.* **2002**, *41*, 3313–3322. (f) Kalsani, V.; Schmittel, M.; Listorti, A.; Accorsi, G.; Armaroli, N. *Inorg. Chem.* **2006**, *45*, 2061–2067. (g) Armaroli, N.; Accorsi, G.; Cardinali, F.; Listorti, A. *Top. Curr. Chem.* **2007**, *280*, 69–115. (h) Iwamura, M.; Takeuchi, S.; Tahara, T. *J. Am. Chem. Soc.* **2007**, *129*, 5248–5256. (i) Iwamura, M.; Watanabe, H.; Ishii, K.; Takeuchi, S.; Tahara, T. *J. Am. Chem. Soc.* **2011**, *133*, 7728–7736. (7) Hashimoto, M.; Igawa, S.; Yashima, M.; Kawata, I.; Hoshino, M.; Osawa, M. *J. Am. Chem. Soc.* **2011**, *133*, 10348–10351. (8) Hoshino, M.; Sonoki, H.; Miyazaki, Y.; Iimura, Y.; Yamamoto, K. *Inorg. Chem.* **2000**, *39*, 4850–4857. (9) Osawa, M.; Kawata, I.; Igawa, S.; Hoshino, M.; Fukunaga, T.; Hashizume, D. *Chem.—Eur. J.* **2010**, *16*, 12114–12126. (10) Burla, M. C.; Caliendo, R.; Camalli, M.; Carrozzini, B.; Cascarano, G. L.; De Caro, L.; Giacovazzo, C.; Polidori, G.; Spagna, R. *J. Appl. Crystallogr.* **2005**, *38*, 381–388. (11) Parr, R. G.; Yang, W. *Density-functional Theory of Atoms and Molecules*; Oxford University Press: Oxford, U.K., 1994. (12) (a) Perdew, J. P. *Electronic Structure of Solids*; Akademie Verlag: Berlin, 1991; pp 10–20. (b) Perdew, J. P.; Chevary, J. A.; Vosko, S. H.; Jackson, K. A.; Pederson, M. R.; Singh, D. J.; Fiolhais, C. *Phys. Rev. B: Condens. Matter* **1992**, *46*, 6671–6687. (c) Perdew, J. P.; Wang, Y. *Phys. Rev. B* **1992**, *45*, 13244–13249. (d) Becke, A. D. *J. Chem. Phys.* **1993**, *98*, 5648–5652. (13) Hay, P. J.; Wadt, W. R. *J. Chem. Phys.* **1985**, *82*, 270–283. (14) (a) Cancès, E.; Mennucci, B.; Tomasi, J. *J. Chem. Phys.* **1997**, *107*, 3032–3041. (b) Mennucci, B.; Cancès, E.; Tomasi, J. *J. Phys. Chem. B* **1997**, *101*, 10506–10517. (15) Miertus, S.; Scrocco, E.; Tomasi, J. *Chem. Phys.* **1981**, *55*, 117–29. (16) Frisch, M. J.; Trucks, G. W.; Schlegel, H. B.; Scuseria, G. E.; Robb, M. A.; Cheeseman, J. R.; Montgomery, J. A., Jr.; Vreven, T.; Kudin, K. N.; Burant, J. C.; Millam, J. M.; Iyengar, S. S.; Tomasi, J.; Barone, V.; Mennucci, B.; Cossi, M.; Scalmani, G.; Rega, N.; Petersson, G. A.; Nakatsuji, H.; Hada, M.; Ehara, M.; Toyota, K.; Fukuda, R.; Hasegawa, J.; Ishida, M.; Nakajima, T.; Honda, Y.; Kitao, O.; Nakai, H.; Klene, M.; Li, X.; Knox, J. E.; Hratchian, H. P.; Cross, J. B.; Bakken, V.; Adamo, C.; Jaramillo, J.; Gomperts, R.; Stratmann, R. E.; Yazyev, O.; Austin, A. J.; Cammi, R.; Pomelli, C.; Ochterski, J. W.; Ayala, P. Y.; Morokuma, K.; Voth, G. A.; Salvador, P.; Dannenberg, J. J.; Zakrzewski, V. G.; Dapprich, S.; Daniels, A. D.; Strain, M. C.; Farkas, O.; Malick, D. K.; Rabuck, A. D.; Raghavachari, K.; Foresman, J. B.; Ortiz, J. V.; Cui, Q.; Baboul, A. G.; Clifford, S.; Cioslowski, J.; Stefanov, B. B.; Liu, G.; Liashenko, A.; Piskorz, P.; Komaromi, I.; Martin, R. L.; Fox, D. J.; Keith, T.; Al-Laham, M. A.; Peng, C. Y.; Nanayakkara, A.; Challacombe, M.; Gill, P. M. W.; Johnson, B.; Chen, W.; Wong, M. W.; Gonzalez, C.; Pople, J. A. *Gaussian 03*, revision D.01; Gaussian, Inc.: Wallingford, CT, 2004. (17) Frisch, M. J.; Trucks, G. W.; Schlegel, H. B.; Scuseria, G. E.; Robb, M. A.; Cheeseman, J. R.; Scalmani, G.; Barone, V.; Mennucci, B.; Petersson, G. A.; Nakatsuji, H.; Caricato, M.; Li, X.; Hratchian, H. P.; Izmaylov, A. F.; Bloino, J.; Zheng, G.; Sonnenberg, J. L.; Hada, M.; Ehara, M.; Toyota, K.; Fukuda, R.; Hasegawa, J.; Ishida, M.; Nakajima, T.; Honda, Y.; Kitao, O.; Nakai, H.; Vreven, T.; Montgomery, H. A., Jr.; Peralta, J. E.; Ogliaro, F.; Bearpark, M.; Heyd, J. J.; Brothers, E.; Kudin, K. N.; Staroverov, V. N.; Kobayashi, R.; Normand, J.; Raghavachari, K.; Rendell, A.; Burant, J. C.; Iyengar, S. S.; Tomasi, M.; Cossi, N.; Rega, J. M.; Millam, M.; Klene, J. E.; Knox, J. B.; Cross, V.; Bakken, C.; Adamo, J.; Jaramillo, J.; Gomperts, R.; Stratmann, R. E.; Yazyev, O.; Austin, A. J.; Cammi, R.; Pomelli, C.; Ochterski, J. W.; Martin, R. L.; Morokuma, K.; Zakrzewski, V. G.; Voth, G. A.; Salvador, P.; Dannenberg, J. J.; Dapprich, S.; Daniels, A. D.; Farkas, O.; Foresman, J. B.; Ortiz, J. V.; Cioslowski, J.; Fox, D. J. *Gaussian 09*, revision A.02; Gaussian, Inc.: Wallingford, CT, 2009.

- (18) (a) Martin, R. L. *J. Chem. Phys.* **2003**, *118*, 4775–4777.
(b) Dreuw, A.; Head-Gordon, M. *Chem. Rev.* **2005**, *105*, 4009–4037.
- (19) (a) Batista, E. R.; Martin, R. L. *J. Phys. Chem. A* **2005**, *109*, 3128–3133. (b) Batista, E. R.; Martin, R. L. *J. Phys. Chem. A* **2005**, *109*, 9856–9859. (c) Kawata, I.; Nitta, H. *J. Chem. Phys.* **2012**, *136*, 640109-1–640109-9.
- (20) Dennett, J. N. L.; Gillon, A. L.; Heslop, K.; Hyett, D. J.; Fleming, J. S.; Lloyd-Jones, C. E.; Orpen, A. G.; Pringle, P. G.; Wass, D. F.; Scutt, J. N.; Weatherhead, R. H. *Organometallics* **2004**, *23*, 6077–6079.
- (21) Zank, J.; Schier, A.; Schmidbaur, H. *J. Chem. Soc., Dalton Trans.* **1999**, 415–420.
- (22) (a) Fife, D. J.; Morse, K. W.; Moore, W. M. *J. Photochem.* **1984**, *24*, 249–263. (b) Kutal, C. *Coord. Chem. Rev.* **1990**, *99*, 213–252.
- (23) Accorsi, G.; Armaroli, N.; Delavaux-Nicot, B.; Kaeser, A.; Holler, M.; Nierengarten, J.-F.; Degli Esposti, A. *J. Mol. Struct. (THEOCHEM)* **2010**, *962*, 7–14.
- (24) (a) Youinou, M. T.; Ziessel, R.; Lehn, J. M. *Inorg. Chem.* **1991**, *30*, 2144–2148. (b) Federlin, P.; Kern, J. M.; Rastegar, A.; Dietrich-Buchecker, C.; Marnot, P. A.; Sauvage, J. P. *New J. Chem.* **1990**, *14*, 9–12.